Tracking the continuous spin-flop transition in Ni_{3}TeO_{6} by infrared spectroscopy

Michael O. Yokosuk, Sergey Artyukhin, Amal al-Wahish, Xueyun Wang, Junjie Yang, Zhiqiang Li, Sang-Wook Cheong, David Vanderbilt, and Janice L. Musfeldt

Phys. Rev. B **92**, 144305 — Published 8 October 2015

DOI: 10.1103/PhysRevB.92.144305

Tracking the continuous spin-flop transition in Ni_3TeO_6 by infrared spectroscopy

Michael O. Yokosuk[1], Sergey Artyukhin[2], Amal al-Wahish[1], Xueyun Wang[2], Juniji Wang[3], Zhiqiang Li[4], Sang-Wook Cheong[2,3], David Vanderbilt[2], Janice L. Musfeldt[1,5]
[1] *Department of Chemistry, University of Tennessee, Knoxville, Tennessee, 37996, USA.*
[2] *Department of Physics and Astronomy and the Rutgers Center for Emergent Materials, Rutgers, The State University of New Jersey, Piscataway, New Jersey 08854, USA.*
[3] *Laboratory for Pohang Emergent Materials and Max Plank POSTECH Center for Complex Phase Materials, Pohang University of Science and Technology, Pohang 790-784, Korea*
[4] *National High Magnetic Field Laboratory, Tallahassee, Florida, 32310, USA. and*
[5] *Department of Physics and Astronomy, University of Tennessee, Knoxville, Tennessee, 37996, USA.*

Easy axis antiferromagnets usually exhibit a first order spin-flop transition when the magnetic field is applied along the easy axis. Recently a colossal magnetoelectric effect was discovered in Ni_3TeO_6, suggesting a continuous spin-flop transition across a narrow phase in this material [Y. S. Oh, *et al.*, Nature Comm. 5, 3201 (2014)]. Additional evidence is, however, desirable to verify this mechanism. Here we measure the infrared vibrational properties of Ni_3TeO_6 in high magnetic fields and demonstrate that the phonon anomalies are consistent with a second-order mechanism.

I. INTRODUCTION

Ni_3TeO_6 sports the largest magnetoelectric effect seen to date in a single-phase material[1] and the second-largest magnetically-induced polarization change.[2] This system has a polar $R3$ structure,[3,4] insulating behavior,[5] and is pyroelectric[1] (Fig. 1). The polarization direction is set by the sequence of Ni and Te ions along the c-axis in the rhombohedral unit cell. Ni ions have the outer shell electronic configuration $t_{2g}^6 e_g^2$ and spin $S = 1$, whereas Te is non-magnetic.[1,4] This system thus provides an opportunity to examine (i) magnetoelectric and magnetoelastic coupling when magnetic order develops in a polar lattice and (ii) how transition metal centers mix with non-magnetic ions that have large spin-orbit coupling. The complex magnetism also provides a framework that motivates the search for new high field phases. Antiferromagnetic ordering sets in at $T_N = 53$ K, with Ni spins along the hexagonal c-axis having $\uparrow\uparrow\downarrow\downarrow\downarrow\uparrow$ ordering in the doubled rhombohedral unit cell (AFM-I)[4]. At the magnetic field of 9 T, applied along the hexagonal c-axis, the spins flop into the ab-plane (AFM-II phase). While most antiferromagnets show a first-order spin-flop transition when the magnetic field is applied along the easy axis,[6–8] Ni_3TeO_6 displays a sequence of two second-order transitions near 9 T limiting a narrow intermediate phase, across which the antiferromagnetic order parameter rotates by a 90° angle.[2] Heisenberg exchange striction in this polar material couples spin canting to the polarization change, giving rise to a colossal magnetoelectric effect in the intermediate phase.[1]

Considering the foundational role of Heisenberg exchange striction in generating spin-lattice coupling, the complex magnetism, and the enormous field-induced polarization changes, direct measurements of the elementary excitations are important for understanding Ni_3TeO_6 and other members of this promising family of compounds.[9–15] Here, we employ infrared vibrational spectroscopy to reveal for the first time the lattice dynamics of Ni_3TeO_6 over a broad range of temperature and magnetic field. Our measurements uncover frequency shifts in the phonons across T_N and through the field-driven spin-flop transition, demonstrating that the lattice is sensitive to changes in the microscopic spin arrangement. Corroborating the measurements with *ab-initio* calculations, we assign infrared absorption peaks, identify phonons that have the largest spin-phonon coupling, and trace the microscopic origin of this coupling. Unexpectedly, spin-lattice coupling in Ni_3TeO_6 involves modes in the ab-plane in addition to those along the c-axis. Both act to modify superexchange. Trends in these features are consistent with the peculiar second order character of the spin-flop transition. Our measurements also reveal signatures of a previously unknown transition between 30 and 35 T that merits additional investigation.

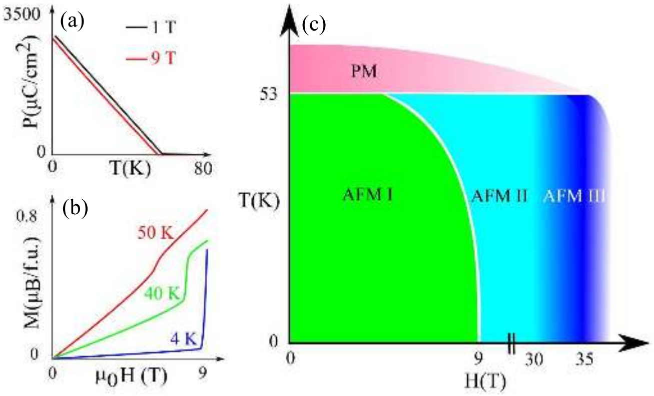

FIG. 1: (a) Temperature dependence of the electric polarization $P_c(H_c)$ showing the magnetically-induced polarization change below the 53 K Néel transition.[1] (b) Magnetization curves at different temperatures.[1] (c) Schematic phase diagram of Ni_3TeO_6 for $H \parallel c$ showing the 9 T spin flop and the possibility of an unexplored transition between 30 and 35 T.

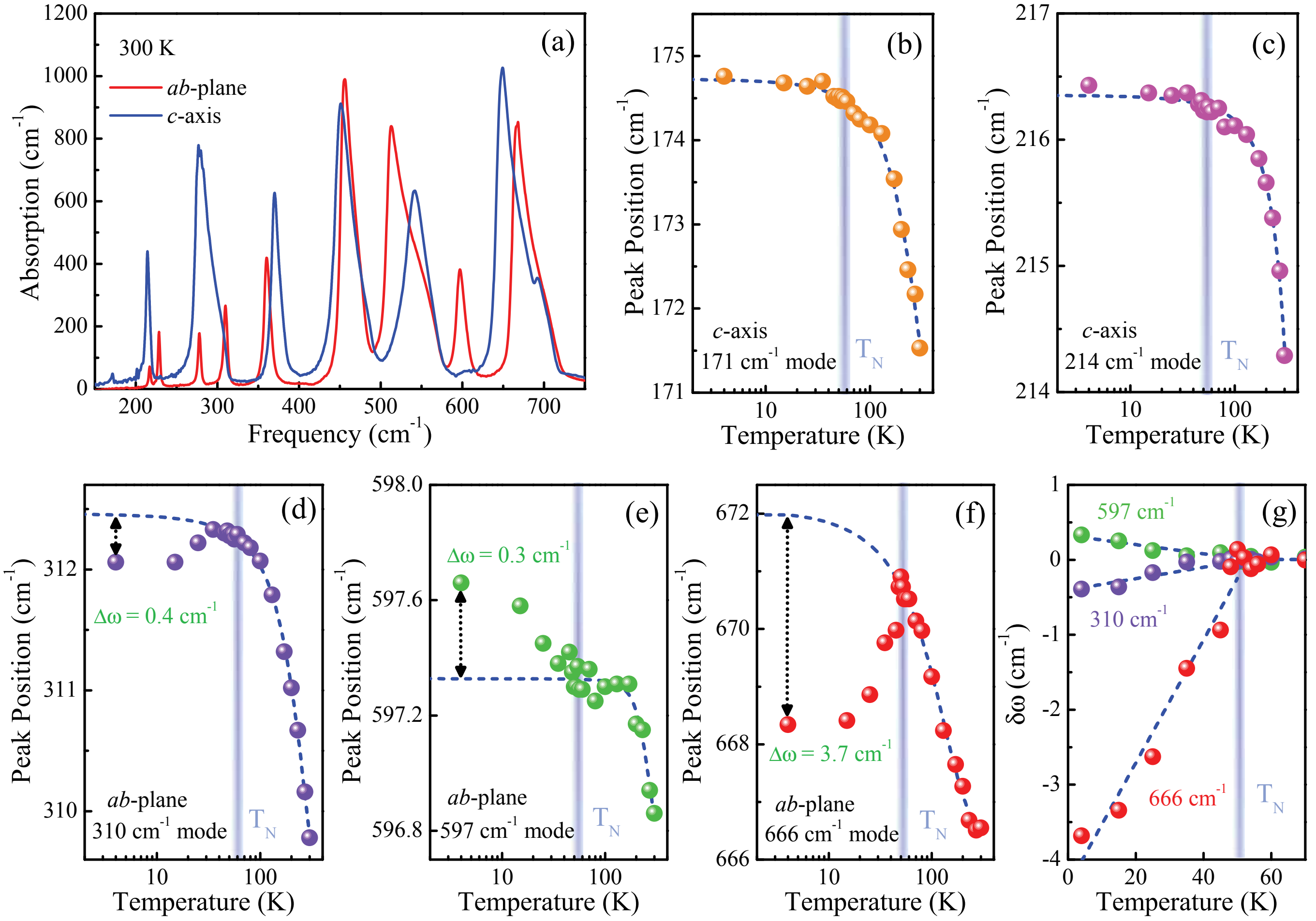

FIG. 2: (a) Polarized infrared absorption spectrum of Ni_3TeO_6 at 300 K. (b-f) Peak position vs. temperature for several characteristic phonons. A Boltzmann sigmoid fit was used to model traditional anharmonic effects, and the difference between the low temperature limit of this model (which gives the unperturbed frequency) and the phonon position at base temperature was used to extract the frequency shifts ($\delta\omega$'s). The Néel temperature is indicated by a vertical line at 53 K. (g) Spin-lattice coupling-induced frequency shifts, $\delta\omega$'s, for the three *ab*-plane phonon modes from panels (d-f), now plotted on a linear temperature scale, together with linear fits.

II. METHODS

Ni_3TeO_6 single crystals were grown by flux techniques as described previously.[1]. Reflectance measurements were performed using a series of spectrometers in the *ab*-plane and along the *c*-axis between 5 and 300 K. A Kramers-Kronig analysis was used to obtain the optical constants. Magneto-infrared experiments employed a polycrystalline sample in either a polyethylene or KBr matrix and a resistive magnet at the National High Magnetic Field Laboratory (100-3000 cm^{-1}; 4.2 K; 0-35 T). The absorption $\alpha(\omega)$ was calculated as $\alpha(\omega) = -\frac{1}{hd} ln(T(\omega))$, where $T(\omega)$ is the measured transmittance, h is the loading, and $\underline{d}$ is the effective thickness. Absorption differences were also calculated in order to highlight small field-induced changes. Here, $\Delta\alpha = \alpha(\omega, H) - \alpha(\omega, H = 0)$. Standard peak fitting techniques were employed as appropriate.

Phonon frequencies were computed using frozen-phonon method as implemented in phonopy and VASP software packages.[16–21] Calculations used generalized gradient approximation within projector-augmented wave formalism[22], plane wave cutoff of 500 eV, 4×4×4 Γ-centered k-point grid, up-up-down spin ordering in a 1×1×1 rhombohedral unit cell. Using a 1×1×2 unit cell where spin exchanges are not frustrated is computationally more expensive, and magnetic field-induced phonon frequency shifts are much smaller than the frequencies themselves, so that a 1×1×1 rhombohedral unit cell seems appropriate for phonon assignment purposes.

III. RESULTS AND DISCUSSION

Figure 2(a) displays the polarized infrared absorption of Ni_3TeO_6 at 300 K. A symmetry analysis predicts 9 E

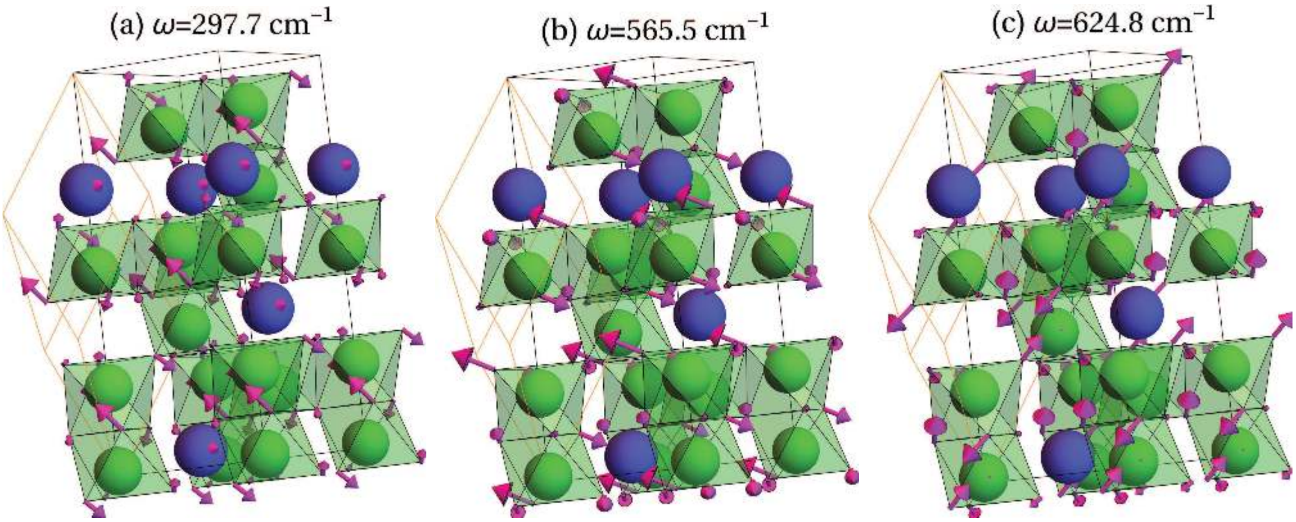

FIG. 3: Displacement patterns for the three characteristic phonons that display large spin-lattice coupling across the Néel transition. Ni and Te ions are shown in green and blue respectively; oxygens (not drawn) are at octahedral vertices. Ionic displacements are are indicated by pink arrows whose length is proportional to the displacement. The rhombohedral unit cell, indicated by the orange lines, contains one Ni_3TeO_6 formula unit.

symmetry optical phonons in the *ab*-plane and 9 optical modes of A symmetry polarized along c ($\Gamma_o = 9E + 9A$). In the polar $R3$ structure,[3,4] the optical modes are both infrared and Raman active.[23] All are present in the infrared response of Ni_3TeO_6 save one, and that mode is observed clearly in the Raman spectrum.[24] The vibrational features are assigned according to our lattice dynamics calculations. A comparison of the theoretically predicted and experimentally observed mode frequencies is shown in Table I along with a description of the displacement patterns. For instance, the phonon at 310 cm^{-1} corresponds to Ni^{I} displacing opposite to Te in the *ab*-plane in a symmetric stretch with Ni^{II} and Ni^{III} remaining at rest. By contrast, the 597 and 666 cm^{-1} modes are octahedral stretching modes, differentiated by the cluster of oxygens that move with respect to the nickel centers (in- vs. out-of-phase oxygen shifts between consecutive planes).

The optical absorption measurements on Ni_3TeO_6 provide microscopic information on the elementary excitations of the lattice. Frequency shifts of these excitations are sensitive probes of structural dynamics, and spin-phonon coupling communicates information on magnetic phase transitions to the structural degrees of freedom. Therefore by tracking the phonon frequencies across the Néel and spin-flop transitions, we can shed the light on the mechanism of spin-lattice coupling.

A. Spin-lattice coupling across the Néel transition

The frequency vs. temperature plots in Fig. 2(b-f) summarize the elastic properties of Ni_3TeO_6 across the 53 K paramagnetic (PM) → AFM-I transition. Three *ab*-plane modes at 310, 597, and 666 cm^{-1} are sensitive to the Néel transition, an indication that lattice behavior is coupled to the magnetic structure. From the displacement patterns in Fig. 3, we see that all these modes involve ionic shifts within the *ab*-plane along with octahedral stretching or bending. Softening of the 666 cm^{-1} stretching mode below T_N is perhaps the clearest change, with a frequency shift of ≈ 3.7 cm^{-1}. If this were a simple binary spin system, then using $\delta\omega = \lambda\langle S_1 \cdot S_2\rangle$ and assuming a limiting low-emperature value of the spin-spin correlation function of $S^2 = 1$ would lead to a spin-lattice coupling constant of the 666 cm^{-1} mode of approximately 3.7 cm^{-1}.[25–27] The coupling constants of the 310 and 597 cm^{-1} modes, 0.4 and 0.3 cm^{-1}, respectively, are estimated in a similar manner (Table I). These spin-lattice coupling constants compare well with those in ferromagnetic $CrSiTe_3$ but are smaller than what is observed in $SrMnO_3$.[28,29] By contrast, spin-lattice coupling in α-$RuCl_3$ manifests primarily as a line width effect.[30] A mean-field analysis of relative slopes of the frequency vs. temperature data near T_N, including an explicit treatment of the multiple sublattices, reveals similar results as discussed below.

The other vibrational modes in Ni_3TeO_6 are insensitive to the magnetic ordering transition, with the peak position vs. temperature data following a sigmoidal Boltzmann curve that captures anharmonicity effects and the temperature dependence of short-range magnetic interactions.[28] Two examples of this behavior are shown in Fig. 2(b, c). Clearly the c-directed 171 and 214 cm^{-1} shearing displacements do not display spin-lattice coupling. The rigidity of these (and other) c-directed modes is somewhat unexpected since the macroscopic polarization develops in this direction. The local lattice distortions in the *ab*-plane induced by the magnetic ordering, and the manner in which the displacements modify the

TABLE I: Phonon frequencies obtained from DFT calculations ($U = 8$ eV), experimental mode frequencies, mode symmetries, spin-lattice coupling constants (the λ's in the text), and displacement patterns. The mode description in the final column encodes shifts of the three Ni ions and the Te center in the sequence Ni^{I}-Ni^{II}-Ni^{III}-Te. u/d = shifts up/down along the c axis; l/r = motion to the left/right in the ab-plane; "-" indicates almost no displacement; octahedral distortions (compression/extension along certain axis/in plane) and rotations are also indicated.

Theoretical Frequencies (cm^{-1})	Experimental Frequencies (cm^{-1})	Mode Symmetries	Coupling Constants (cm^{-1})	Mode Displacement Patterns
167	171	A	–	uudd
205	214	A	–	udud
209	217	E	–	lrrl
217	228	E	–	lrlr
264	278	A	–	-ddu
265	278	E	–	llrr, oct rot around a(b)
297	310	E	0.4	l–r, oct rot
343	360	E	–	oct compression ab
353	370	A	–	udud oct compr c
399	–	A	–	oct twist
425	456	E	–	oct compr ab+twist
426	451	A	–	d-dd+oct twist
488	513	E	–	oct twist ab
512	541	A	–	oct contr c+rot c
562	597	E	0.3	oct contr a(b)
601	649	A	–	oct axial stretching
622	666	E	3.7	oct contr a+b(a-b)
653	692	A	–	oct asymmetric stretching

super-exchange interactions between the magnetic centers and break inversion symmetry, clearly play a much more important role.

A generic Hamiltonian for a phonon mode with a coordinate q, mass m and frequency w is given by

$$H = \frac{p^2}{2m} + \frac{m\omega^2 q^2}{2} + \sum_{ij} \left(q\alpha_{ij} + \frac{q^2}{2}\gamma_{ij} \right) \vec{S}_i \cdot \vec{S}_j + \frac{\beta q^4}{4}, \tag{1}$$

where the first two terms are the kinetic and potential energy in the paramagnetic state, the term with α_{ij} describes the force on q due to Heisenberg exchange striction, and the term with γ_{ij} – the spin-dependent part of the mode stiffness.[31] As a result of magnetic ordering, the mode frequency will shift due to two reasons: (i) the stiffness will change due to the γ_{ij} term and the force described by the α_{ij} term will shift the equilibrium position to q_0, and (ii) the anharmonic effects (term with β) will further shift the frequency. One can obtain the frequency shift by substituting $q = q_0 + \delta q$, and completing the full square in δq we obtain for the phonon frequency shift to the linear order in small α_{ij} and γ_{ij}:

$$\delta\omega = \frac{1}{2m} \left(\Gamma + \frac{3\beta A}{2m\omega^2} \right), \tag{2}$$

where we denote

$$A = \sum_{ij} \alpha_{ij} \vec{S}_i \cdot \vec{S}_j \tag{3}$$

$$\Gamma = \sum_{ij} \gamma_{ij} \vec{S}_i \cdot \vec{S}_j. \tag{4}$$

Above the Néel temperature $\vec{S} = 0$, while below the ordered magnetic moments grow with some critical exponent $S \sim (T_c - T)^{\nu}$. That leads to $A \sim \Gamma \sim (T_c - T)^{2\nu}$.

Since the frequency shift away from normal temperature trends due to anharmonicity and short-range magnetic interactions is related to the square of the order parameter, plots of $\delta\omega$ vs. temperature provide insight into the nature of the ordering transition. The 666 cm^{-1} NiO_6 stretching mode is most revealing in this regard. To test the predictions outlined above, we fit the experimental frequency shift $\delta\omega$ as $\alpha(\mathrm{T}_c - \mathrm{T})^{2\nu}$. The results for all three of the ab-plane phonons that engage in spin-lattice coupling through T_N are shown in Fig. 2(g). We immediately observe the linear $\delta\omega$ vs. temperature relationships and exponents of 2ν that are very close to 1.0. This is consistent with expectations for a continuous second order transition. The coupling is strongest for the 666 cm^{-1} mode with $\alpha = 8 \times 10^{-2}$ cm^{-1}/K. The 310 and 597 cm^{-1} modes have α's of 8×10^{-3} and 6×10^{-3}

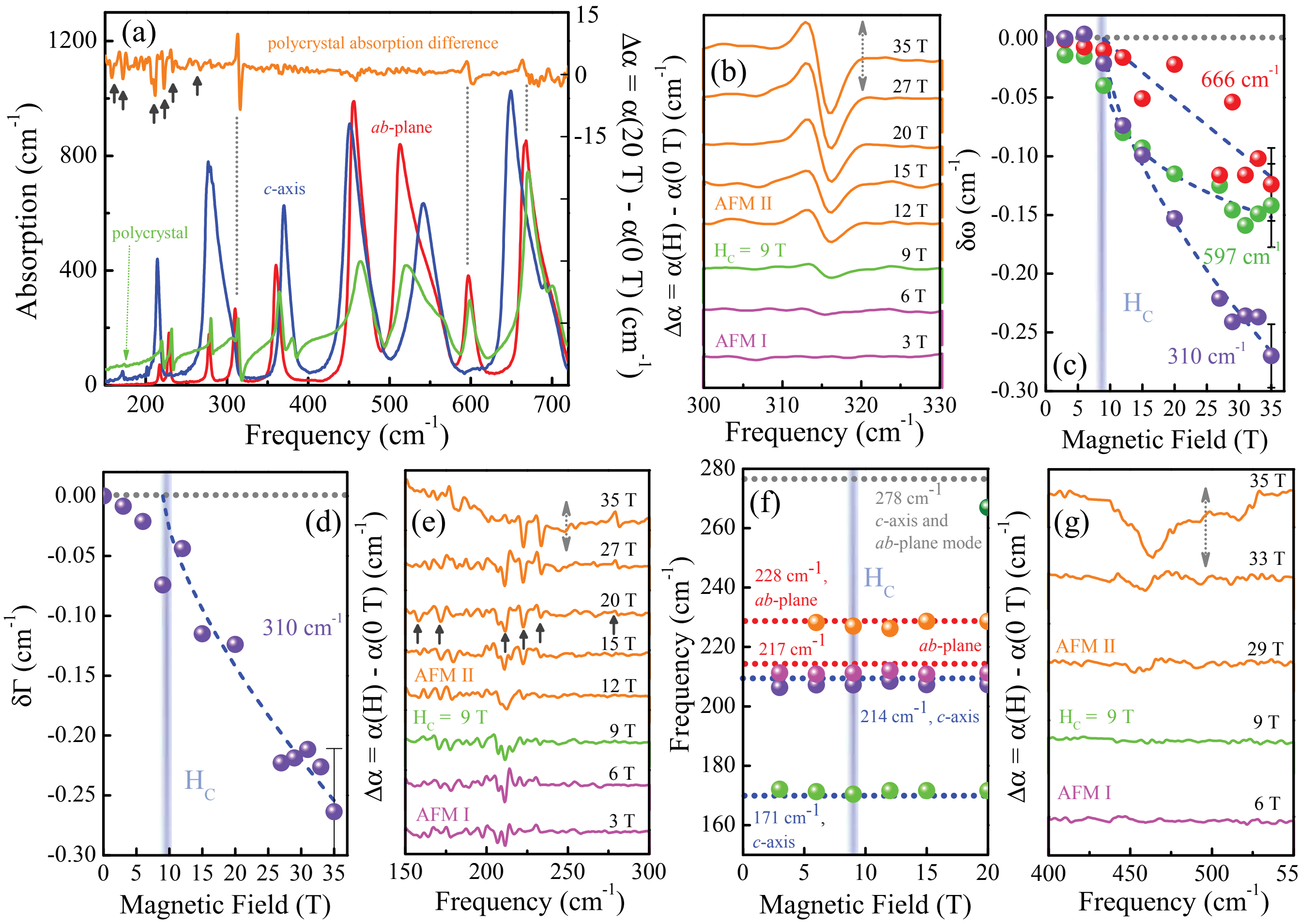

FIG. 4: (a) Polarized infrared absorption spectrum, the polycrystal response, and the absorption difference spectrum at 20 T. The latter highlights the changes in the local lattice distortions between the AFM I and AFM II phases and is defined as $\Delta\alpha = \alpha(\omega, H) - \alpha(\omega, H = 0)$. (b, c, d) Close-up view of the field-induced absorption difference spectrum in the vicinity of the 310 cm^{-1} mode through the 9 T spin flop transition along with the field-induced frequency shift and line width changes. The curves in (b) are offset by 80 cm^{-1} for clarity, and the dotted arrow is a 20 cm^{-1} scale bar. The vertical line in (c, d) indicates the 9 T critical field. (e, f) Close-up view of the field-induced absorption difference spectra in the vicinity of the most collective vibrational modes along with a contour plot revealing the subtle frequency shifts through the spin flop transition. The curves in (e) are offset by 80 cm^{-1}, and a 20 cm^{-1} scale bar is included. (g) Waterfall plot in the vicinity of the 451 and 456 cm^{-1} modes providing evidence for an unexplored transition between 30 and 35 T. Each curve in the waterfall plot is offset by 85 cm^{-1}, and the scale bar is 20 cm^{-1}. All data was taken at 4.2 K.

cm^{-1}/K, respectively.[32] When one multiplies by an appropriate temperature scale such as T_N, these α's are in good agreement with the aforementioned λ's.

As we can see from the size of the coupling constants, the 666 cm^{-1} mode dominates spin-lattice coupling through the 53 K Neél transition. This mode compresses the octahedra in the *ab* plane with out-of-phase motion between consecutive planes.[33] The latter is essentially an antiphase accordion-like pattern that modulates super-exchange between Ni^{I} and Ni^{II} in the *c* direction. This aspect of the inter-plane motion reinforces the development of the remarkable low temperature polarization.

A Kramers-Kronig analysis of the measured reflectance also provides the frequency dependent dielectric response of Ni$_3$TeO$_6$, which we can extrapolate to zero frequency for comparison with the permittivities reported in Ref. 1. Just above T_N, we find $\epsilon_1(0) = 7.6$ in the *ab*-plane, typical of a magnetic oxide, whereas $\epsilon_1(0)$ is 6.5 at 4.2 K. The difference is 1.1. The noise level is much larger in the *c*-direction. Here, we find that ϵ_1 is approximately 17.2 near T_N and about 16 at 4.2 K, giving $\Delta\epsilon_1 = 1.2$ within our sensitivity. These values of ϵ_1 are in reasonable agreement with the size and temperature dependence of the dielectric constant reported previously,[1] suggesting that there will be limited dispersion between the THz and MHz regimes.

B. Spin-lattice coupling through the field-driven spin flop transition

We can more deeply examine the role of Heisenberg exchange striction in generating spin-lattice interactions by investigating the magnetic field-driven AFM I → AFM II spin-flop transition. Analogous to the temperature-driven PM → AFM I transition that was modeled as $A \sim \Gamma \sim (T_c - T)^{2\nu}$ in Fig. 2(g), the magnetization is predicted to grow from zero as $(H - H_c)^{\mu}$ at a second-order spin-flop transition. Therefore A and Γ acquire analogous contributions, growing as $(H - H_c)^{2\mu}$. This according to Eq. 2 leads to $\delta\omega \sim (H - H_c)^{2\mu}$, and a cusp in $\delta\omega(H)$ should be observed. In the case of a first-order phase transition, magnetization should emerge in a jump-like fashion, and therefore a sudden jump is expected in $\delta\omega$. Furthermore, the jump must be hysteretic. This scenario describes a traditional spin-flop transition such as that found in hematite.[6,34,35] A second-order transition will be different in that field-induced frequency shifts and line width modifications should be continuous. We test these ideas against the behavior of several representative phonons below.

Figure 4(a) displays the magneto-infrared response of Ni_3TeO_6, $\Delta\alpha = [\alpha(H = 20\text{ T})$ - $\alpha(H = 0\text{ T})]$, along with the linear absorption for comparison. Several phonons are sensitive to changes in the microscopic spin pattern across the 9 T transition. The absorption difference spectrum reveals a number of small, sharp structures below 280 cm^{-1} along with larger derivative-like features that correspond to modifications of the 310, 597, and 666 cm^{-1} modes. While the latter correspond to changes in the familiar E symmetry vibrational modes (polarized in the ab-plane), the structures below 280 cm^{-1} arise from both ab-plane and c-polarized structures with E and A symmetries, respectively (Table I). No spectral hysteresis is observed, consistent with expectations for a non-hysteretic transition.

Figure 4(b) shows a close-up view of the field-induced absorption difference in the vicinity of the 310 cm^{-1} mode. A clear derivative-like structure develops above 9 T in the $\Delta\alpha$ spectrum. Driving through the spin flop transition modifies both frequency and linewidth - different from the trends across the 53 K Néel transition. The field-induced frequency shift and change in line width extracted from an analysis of the 310 cm^{-1} feature are shown in Fig. 4(c, d). We find that $\delta\omega$ is rigid in the AFM I phase whereas it softens with increasing field in AFM II. The latter trend is fit as $\delta\omega \sim (H - H_c)^{2\mu}$. Although the number of points in the vicinity of H_c is not enough to precisely determine the critical exponent, there is no characteristic first-order jump. The 597 and 666 cm^{-1} modes display similar behavior, although the error bars are larger. Likewise, the linewidth is relatively constant in the AFM I phase whereas it narrows with increasing field in AFM II. A fit to $\delta\Gamma \sim (H - H_c)^{2\mu}$ again yields a reasonable match (within error bars), in line with expectations for a continuous phase transition.

The absorption difference spectrum in Fig. 4(a) also reveals a great deal of low frequency fine structure. These features are indicated by arrows. The majority correspond to changes in the 171, 214, 217, 228, and 278 cm^{-1} fundamentals, although the 158 cm^{-1} structure, for example, is new. Figure 4(e) shows a close-up view of how these features change with magnetic field, and Fig. 4(f) diagrams the development of the magneto-infrared contrast in a more graphical way, pointing out the extent to which applied field modifies a particular feature. The zero-field phonon frequencies are indicated with horizontal dotted lines for comparison. All of these modes involve displacements of the Ni and Te centers that alter the magnetic exchange pathway between the Ni centers. Remembering that polarization is along c, these shifts of the magnetic centers along with the movement of Te ions and oxygen octahedra contribute to altering the magnetic exchange pathway and furthermore the polarization. The intermediate phase, across which the antiferromagnetic order parameter rotates continuously by 90 degrees, is narrow, and present measurements do not resolve it.

The magneto-infrared spectra also reveal the possibility of an additional, as yet unexplored, transition between 30 and 35 T. Figure 4(g) displays the strongest evidence for this crossover, although the absorption difference curves in Fig. 4(e) show additional fine structure developing in this regime as well. These changes correlate well with a slope change in the high field magnetization,[2] which presumably corresponds to an important rotation or canting of the spin. Alternately, the high field transition may be related to elongation of the unit cell. In this scenario, zone folding will activate zone boundary modes - in addition to narrowing the 451 and 456 cm^{-1} features. For illustrative purposes, we include this transition in the schematic phase diagram of Fig. 1(c). Spin-lattice interactions between 30 and 35 T are probably just a prelude to more dramatic property changes at 57 T.[2]

IV. CONCLUSION

Summarizing, vibrational property measurements were brought together with complementary first principles lattice dynamics calculations and a mean field analysis to uncover the elastic properties of Ni_3TeO_6 across the Néel and spin flop transitions. Our analysis unexpectedly reveals that the 666 cm^{-1} in-plane octahedral stretching mode is most sensitive to the 53 K magnetic ordering transition, a finding that we discuss in terms of modified superexchange interactions between Ni^{I} and Ni^{II} as well as the development of the sizable polarization. At the same time, magneto-infrared spectroscopies demonstrate the gradual evolution of a number of modes across the 9 T spin flop transition, consistent with a continuous second-order mechanism and quite distinct from expectations for a first-order process. We also provide evidence for a previously unexplored transition between 30 and 35 T. These findings reveal another aspect of magnetoelectric coupling and are important for understanding the development of large, controllable responses in Ni_3TeO_6 and other multifunctional materials.

Acknowlegments

Research at the University of Tennessee and Rutgers University was supported by the NSF-DMREF program under DMR-1233118 and DMR-1233349. D.V. and S.A. also acknowledge the partial support through the ONR grant N00014-12-1-1035. Work at Postech is funded by the Max Planck POSTECH/KOREA Research Initiative Program 2011-0031558 through NRF of Korea funded by MEST. A portion of this work was performed at the National High Magnetic Field Laboratory, which is supported by the National Science Foundation Cooperative Agreement DMR-1157490, the State of Florida, and the U.S. Department of Energy.

---

[1] Y. S. Oh, S. Artyukhin, J. J. Yang, V. S. Zapf, J. W. Kim, D. Vanderbilt, and S. -W. Cheong, Nat. Commun. **5**, 3201 (2014).

[2] J. W. Kim, S. Artyukhin, E. D. Mun, M. Jaime, N. Harrison, A. Hansen, J. J. Yang, Y. S. Oh, D. Vanderbilt, V. S. Zapf, and S. -W. Cheong submitted to Phys. Rev. Lett.

[3] R. Becker and H. Berger. Acta Cryst. **E62**, i222 (2006).

[4] I. Živković, K. Prša, O. Zaharko, and H. Berger J. Phys.: Condens. Matter **22**, 056002 (2010).

[5] M. O. Yokosuk, A. al-Wahish, S. Artyukhin, D. Mazumdar, P. Chen, K. R. O'Neal, J. Yang, Y. S. Oh, S. A. McGill, K. Haule, D. Vanderbilt, S.-W. Cheong, and J. L. Musfeldt, in preparation.

[6] T. Kaneko and S. Abe, J. Phys. Soc. Japan **20**, 2001 (1965).

[7] A. N. Bogdanov, A. V. Zhuravlev, and U. K. Rössler, Phys. Rev. B. **75**, 094425 (2007).

[8] V. V. Eremenko, N. É. Kaner, Y. G. Litvinenko, and V. V. Shapiro, Sov. Phys. JETP **62**, 746 (1985).

[9] J. H. Kim and J. H. Han, Phys. Rev. B. **76**, 054431 (2007).

[10] U. Adem, M. Mostovoy, N. Bellido, A. A. Nugroho, C. Simon, and T. T. M. Palstra, J. Phys.: Condens. Matter **21**, 496002 (2009).

[11] H. J. Xiang, E. J. Kan, S.-H. Wei, M.-H. Whangbo, and X. G. Gong, Phys. Rev. B. **84**, 224429 (2011).

[12] T. Katsufuji, S. Mori, M. Masaki, Y. Moritomo, N. Yamamoto, and H. Takagi, Phys. Rev. B. **64**, 104419 (2001).

[13] C. dela Cruz, F. Yen, B. Lorenz, Y. Q. Qang, Y. Y. Sun, M. M. Gospodinov, and C. W. Chu, Phys. Rev. B. **71**, 060407(R) (2005).

[14] J. E. Hamann-Borrero, S. Partzsch, S. Valencia, C. Mazzoli, J. Herrero-Martin, R. Feyerherm, E. Dudzik, C. Hess, A. Vasiliev, L. Bezmaternykh, B. Büchner, and J. Geck, Phys. Rev. Lett. **109**, 267202 (2012).

[15] H. N. Li, J. W. Huang, L. X. Ziao, L. P. Peng, Y. Y. Wu, G. H. Du, Z. W. Ouyang, B. R. Chen, and Z. C. Xia, J. Appl. Phys. **111**, 083913 (2012).

[16] A. Togo, F. Oba, and I. Tanaka, Phys. Rev. B. **78**, 134106 (2008).

[17] G. Kresse and J. Hafner, Phys. Rev. B. **47**, 558 (1993).

[18] G. Kresse and J. Hafner, Phys. Rev. B. **49**, 14251 (1994).

[19] G. Kresse and J. Hafner, Comput. Mat. Sci. **6**, 15 (1996).

[20] G. Kresse and J. Furthmüller, Phys. Rev. B. **54**, 11169 (1996).

[21] P. E. Blöchl, Phys. Rev. B. **50**, 17953 (1994).

[22] PAW_GGA Ni_pv 19Apr2000; PAW_GGA Te 07Sep2001; PAW_GGA O 05Jan2001.

[23] G. Blasse and W. Hordijk, J. Solid State Chem. **5**, 395 (1972).

[24] J. G. Cherian, in preparation.

[25] C. J. Fennie and K. M. Rabe, Phys. Rev. Lett. **96**, 205505 (2006).

[26] T. Rudolf, Ch. Kant, F. Mayr, J. Hemberger, V. Tsurkan and A. Loidl, Phys. Rev. B. **76**, 174307 (2007).

[27] A. B. Sushkov, O. Tchernyshyov, W. Ratcliff II, S.-W. Cheong and H. D. Drew, Phys. Rev. Lett. **94**, 137202 (2005).

[28] L. D. Casto, A. J. Clune, M. O. Yokosuk, J. L. Musfeldt, T. J. Williams, H. L. Zhuang, M.-W. Lin, K. Xiao, R. G. Hennig, B. C. Sales and D. Mandrus, APL Materials **3**, 041515 (2015).

[29] S. Kamba, V. Goian, V. Skoromets, J. Hejtmánek, V. Bovtun, M. Kempa, F. Borodavka, P. Vaněk, A. A. Belik, J. H. Lee, O. Pacherová and K. M. Rabe, Phys. Rev. B. **89**, 064308 (2014).

[30] L. J. Sandilands, Y. Tian, K. W. Plumb, Y.-J. Kim, and K. S. Burch, Phys. Rev. Lett. **114**, 147201 (2015).

[31] We assume a phonon irrep for which q^3 terms vanish by symmetry.

[32] Examination of the displacement patterns in Fig. 3 reveals that all three modes either shift the Ni^I center or modify the environment around Ni^I and Ni^{II}. The magnetic interaction between these centers is strong because the octahedra share edges.

[33] This is different from the 597 cm^{-1} mode which also modulates the octahedra and has an in-phase relationship between consecutive layers.

[34] S. Foner and Y. Shapira, Phys. Lett. A. **29**, 276 (1969).

[35] Y. Shapira, Phys. Rev. **184**, 589 (1969).